Title: Mechanical Properties and Fatigue Responses of Fiber Metal Nanocomposite Laminates with Double-Edged Cracks

Authors: Ming-Hwa R. Jen, Li-Jen Hsu, Yu-Cheng Liang, Ying-Hui Wu

Affiliation: Department of Mechanical and Electro-Mechanical Engineering, National Sun Yat-Sen University

Address: 70, Lien-hai Road, Gushan District, Kaohsiung, 80424, Taiwan, ROC.

Corresponding Author: Professor Ming-Hwa R. Jen

Correspondent: jmhr@mail.nsysu.edu.tw

Tel: +886-7-5252000 ext. 4216

Fax: +886-7-5254299

Mechanical Properties and Fatigue Responses of Fiber Metal Nanocomposite Laminates with Double-Edged Cracks

Abstract

The fiber metal laminates (FMLs) of both Ti/APC-2 neat and nanocomposite laminates were fabricated. The double-edged cracks of both symmetry and anti-symmetry were cut in FMLs. From tensile tests we received the load vs. displacement curves and mechanical properties. From cyclic tests the load vs. cycles (P-N) curves, residual life, and failure mechanisms were obtained. The mechanical properties of symmetrically cracked specimens were slightly lower than those of anti-symmetrically cracked counterparts. As the crack length increasing and inclined angle decreasing, the fatigue life decreased. The enhancement of nano-powder improved the ultimate load and fatigue life. The local stress intensity at the crack tip dominates the fatigue responses. The piece of elliptical part was observed from cyclic tests at failure. Although the attraction of two crack tips accelerated the crack growth rate, however, the delay to failure was caused by forming a small piece of ellipse centrally.

Keywords: Double edge notch specimens, Fatigue, Fracture, Hybrid bonding, Nanostructures.

NOMENCLATURE

a Crack length
a^* The shortest distance between the midpoint of two cracks
B Thickness of FMLs
W Width of sample
K_I Stress intensity factor of mode I
K_{II} Stress intensity factor of mode II
K_C Critical value of stress intensity factor of mixed mode
K_I^0 The revised results of stress intensity factor of mode I
K_{II}^0 The revised results of stress intensity factor of mode II
ΔK_e Effective revised stress intensity factor range

θ Inclined angles

1. INTRODUCTION

The fiber metal laminates (FMLs) are, hybrid composite structures, fabricated of thin metallic alloys sheets sandwiched by fiber-reinforced polymeric composites laminates. Due to cyclic loads the fatigue life of FMLs is similar to that of conventional metallic materials and can be classified into three stages such as crack initiation, slow and stable crack growth and rapidly unstable crack growth to final failure. It is well-known the dominant fatigue life of the metals is on the first stage of crack initiation, thus, the demand of quality control is required. However, for FMLs the research of fatigue life is focused on the second stage of stable crack propagation. To describe the metal sheet crack growth, composites matrix cracking, delamination and fibers broken in FMLs the cracking behavior is rather complex, coupled with the stress bridging from the cracked metal sheets into intact fibers. Hence, the difference between the predicted life and the experimental data is reasonably expected.

In the consideration of green material FMLs such as Ti/APC-2 with thermoplastic matrix, instead of thermal-setting matrix, offer superior resistance to severe environmental conditions such as high temperature [1], strong bonding capability without delamination in services, high resistance to impact and cyclic loadings, especially in excellent fatigue resistance and durability [2, 3]. The stress bridging mechanism in the interfaces [4] results in the retardation of crack growth rate in FMLs. The FMLs may still sustain the capability to carry the applied loads even after the failure of through-the-width metal fracture [5-7]. That is unreachable for conventional monolithic materials.

Generally, the FMLs has been originally developed in the aircraft industry and found the application in the fuselage skin of Airbus A380 as an example. Their

favorable fatigue crack growth retardation is significantly beneficial for the cracks to reach considerable length in the relative wide panels. The concept of residual strength can be applied to determine the final failure stage of the structures [8].

From the survey of literature, Gross and Seelig [9] considered the crack initiation, growth rate and direction to provide the methods in fracture mechanics to solve the problems of double-edge-cracked composite laminates subjected to both tensile and fatigue loadings.

In the mixed modes of I/II and I/III Aliha et al. [10] studied the crack initiation behavior of varied polyurethane foams. Alderliesten [11] proposed an analytical model for crack propagation of through-thickness cracks in FMLs due to constant-amplitude cyclic loadings. Guo et al. [12] suggested a way to determine the stress intensity factor (SIF) at the crack tip of metal layers by using the far-field stresses and presence of bridging stresses. Chang and Yang [13] predicted analytically the crack growth rate by adopting an empirical Paris-type equation, whereby the effective SIF of metal layer modulated by the bridging effect. Homan [14] assumed the fatigue crack initiation in FMLs is only dominated by the applied cycles in metal layers and validated by fatigue tests. Gupta [15] showed that crack paths deflect under fatigue loading in FMLs, because the mixed-mode loading presented at the crack tip. Wang et al. [16] presented analysis and numerical simulation on the stress intensity factors for steel plates reinforced with fiber/polymer laminates with double-edge cracks. After a series of tests and adjustments Jen et al. [17] found the optimal amount of nanoparticles (SiO_2) was 1 wt. % in fabricating AS-4/PEEK hybrid laminates. Ilham et al. [18] presented a summary of matrix cracking in nanocomposite materials under the condition of fatigue, tensile, thermal and flexural loadings. Borowski et al. [19] reduced the interlaminar fiber-matrix cracking and delamination in CFRP laminates by adding the multi-walled carbon

nanotubes to improve their fracture toughness.

Based on a series of related research work carbon fiber/thermoplastic matrix AS-4/ PEEK composites sandwiched between Ti alloy sheets were fabricated. The samples with double-edged cracks symmetrically and anti-symmetrically were subjected to tensile and cyclic tests to obtain the mechanical properties, failure mechanisms and fatigue lives. The measured data were compared with the previously obtained data of counterparts with inclined single edge cracks to see the interaction effect of both crack tips of double edged cracks. Also, the found interesting phenomenon of failure forms were illustrated.

2. EXPERIMENTAL

Analytical modelling, numerical simulations and experiments were all concentrated on Ti/APC-2/Ti FMLs. Twelve-inch wide prepregs of CF/PEEK plies were cut and stacked into cross-ply layups. The 0.5 mm thick Ti sheets were optimally treated by chromic acid anodic method of electroplating. The layers of 50-70 μm plating created a strong bonding with $[0/90]_s$ laminates. The hybrid sandwiched three-layer composite laminates were fabricated by using the modified diaphragm curing process, i.e., please refer to the diagrams of pressure and temperature vs. time in [1]. The geometry and dimensions of a plated specimen were 240 mm (length) × 25 mm (width) × 1.55 mm (thickness) as shown in Fig. 1(a), and the samples with double-edged cracks were shown in Fig. 1(b). The cracks were cut by using the electric wire discharge method with the width of 0.3 mm in accordance with ASTM E740-03. For hybrid nanocomposite laminates the nanoparticles of SiO_2 were spread uniformly at the interfaces between 0° and 90° plies with the amount of 1 % by weight.

In performing the tests a servohydraulic computer-controlled dynamic material testing machine, MTS-810,was used to do both static tensile tests and constant stress

amplitude tension-tension cyclic tests with stress ratio of 0.1, at frequency of 5 Hz, and a sinusoidal wave form under the load-controlled mode at room temperature. The 25 mm extensometer, MTS-634.11 F-25, was employed to continuously monitor the strains in the whole testing process of both tests.

For the tensile tests at least 3specimens were used and expressed in average value with standard deviation; while for the cyclic tests more than 6 specimens were performed to construct a load vs. cycles curve by staircase method. The cyclic tests were stopped at a million cycles and denoted by run-outs as small arrows to the right.

3. RESULTS

From the static tensile tests we received the load vs. displacement curves and the mechanical properties for neat and nanocomposite cracked samples of crack lengths 2.0 mm and 3.0 mm at inclined angles ±30°, ±45°, ±60°. The data of 2.0 and 3.0 mm crack lengths were listed. For neat symmetrically double-edge-cracked samples the mechanical properties were presented in Table 1 for $\theta = 30°$, $\theta = 45°$, and $\theta = 60°$ and (a) for 2.0 mm, (b) for 3.0 mm crack length, respectively. Similarly, the mechanical properties for crack length 2.0 mm are expressed in (a) and crack length 3.0 mm in (b) for Tables 2-4. Next, for nanocomposite symmetrically double-edge-cracked samples, their mechanical properties were presented in Table 2 for $\theta = 30°$, $\theta = 45°$, and $\theta = 60°$, respectively. As for neat anti-symmetrically double-edge-cracked samples the mechanical properties by tensile tests were listed in Table 3 for $\theta = 30°$, $\theta = 45°$, and $\theta = 60°$, respectively. As for nanocomposite anti-symmetrically double-edge-cracked samples the mechanical properties were presented in Table 4 for $\theta = \pm 30°$, $\theta = \pm 45°$, and $\theta = \pm 60°$, respectively.

From cyclic tests the P-N curves for neat symmetrically double-edge-cracked samples were shown in Figure 2(a) for crack length 2.0 mm and Figure 2(b) for crack

length 3.0 mm with θ = 30°, 45°, 60° together. The P-N curves for nanocomposite symmetrically double-edge-cracked samples were presented in Figure 3(a) for crack length 2.0 mm and Figure 3(b) for crack length 3.0 mm with θ = 30°, 45°, 60°. Herein, the residual fatigue life is defined as the number of cycles due to applied loading that results in the broken sample with separated pieces. In the comparison of nano-powder SiO_2 improvement, for example, both the P-N curves for neat and nanocomposite anti-symmetrically double-edge-cracked samples were illustrated in Figure 4 for crack length 3.0 mm at $\theta = \pm 45°$. The P-N curves for 2.0 mm and 3.0 mm crack lengths in nanocomposite anti-symmetrically double-edge-cracked samples were represented in Figure 5 for $\theta = \pm 45°$.

4. DISCUSSION

In fabricating Ti/APC-2 nanocomposite laminates the superior and stable mechanical properties of the samples due to tensile tests should be maintained. Based on the rule of mixtures it is found see that the errors were very small between the predicted results and experimental data, i.e., the errors for strength were less than 7.90%, while the errors for stiffness less than 1.48%. That demonstrates the fabricated neat and nanocomposite Ti/APC-2 samples were of good quality and small scatterness after cyclic tests, please refer to [20].

Generally, it is reasonable to predict that the strength, stiffness and life of both neat and nanocomposite laminates, symmetrically and anti-symmetrically double-edge-cracked samples were lower for crack length 3.0 mm in the detrimental situations as illustrated in Tables 1(a) and 1(b) to 4(a) and 4(b). Similarly, the higher the inclined angles are, i.e., $\theta = 60°$ symmetric samples and $\theta = \pm 60°$ for anti-symmetric samples, the higher the mechanical properties and fatigue lives are. That is attributed to the longer distance between the two crack tips. It is also found the mechanical properties

of anti-symmetric samples are slightly better than those of symmetric counterparts. The shortest distance, i.e., show cut, between the two crack tips for the anti-symmetric samples is slightly longer than that of symmetric counterparts.

The addition of nano-powder SiO_2 in the APC-2 interfaces did improve the mechanical properties and cyclic lives, but not significantly. The enhancement of mechanical properties and lives was less than 10%. Some test data showed that the enhancement was even not occurred. It is reasonable to doubt that the enhancement at the crack tips was totally balanced by the crack tip stress intensity factors, i.e., the spreading of nano-powder was global; whilst the stress intensity factor as the crack tip was strongly a local point. That can be explained by the state of crack tip starting from singular point outwards to process zone, plastic zone and sample elastic zone. In FMLs the plastic zone is very small, thus, the enhancement at such a small zone does not effectively improve the mechanical properties and fatigue lives.

For symmetrically double-edge-cracked samples, as shown in Figure 1(b) and Figure 1(c), the stress intensity factors, K_I and K_{II}, in mixed mode can be expressed in Equations (1)-(3), where a is crack length, W denotes the width of sample, and B is thickness of FMLs. The critical value of SIF, K_C, is simply adopted in Equation 4.

$$K_I = \frac{P}{B\sqrt{W}} f\left(\frac{a}{W}\right)\cos^2\theta \tag{1}$$

$$K_{II} = \frac{P}{B\sqrt{W}} f\left(\frac{a}{W}\right)\cos\theta\sin\theta \tag{2}$$

where

$$f\left(\frac{a}{W}\right) = \frac{\sqrt{\frac{\pi a}{2W}}}{\sqrt{1-\frac{a}{W}}}\left[1.122 - 0.561\left(\frac{a}{W}\right) - 0.205\left(\frac{a}{W}\right)^2 + 0.471\left(\frac{a}{W}\right)^3 + 0.190\left(\frac{a}{W}\right)^4\right] \tag{3}$$

$$K_C = \sqrt{K_I^2 + K_{II}^2} \tag{4}$$

Using Equations (1)-(4) the results of K_I , K_{II} and K_C for two crack lengths at each inclined angle were easily obtained. In the consideration of the interaction of two crack tips of symmetrically double-edge-cracked samples the stress intensity factors should be corrected by Equations (5)-(6), where a^* is the shortest distance between the midpoint of two cracks. The revised forms are

$$K_I^0 \approx K_I \left[1 + \frac{a^*}{2d^2} (2\cos 2\varnothing - \cos 4\varnothing) \right] \tag{5}$$

$$K_{II}^0 \approx K_{II} \left[1 + \frac{a^*}{2d^2} (-\sin 2\varnothing + \sin 4\varnothing) \right] \tag{6}$$

The results of stress intensity factors such as K_I^0 and K_{II}^0 were listed in Table 5. Similarly, refer to Figure 1(b) the stress intensity factors can also be easily received for neat and nanocomposite anti-symmetrically double-edge-cracked samples of two crack lengths at each inclined angle. According the interaction of both crack tips as shown in Figure 1(c) the revised results of stress intensity factors such as K_I^0 and K_{II}^0 for those samples can be calculated by using Equations (7)-(8), and the values are tabulated in Table 6, where a^* = 1.0 mm for crack length a = 2.0 mm and a^* = 1.5 mm for a = 3.0 mm.

$$K_I^0 \approx K_I \left[1 + \frac{a^{*2}}{2d^2} (2\cos 2\varnothing - \cos 4\varnothing) \right] \tag{7}$$

$$K_{II}^0 \approx K_{II} \left[1 + \frac{a^{*2}}{2d^2} (-\sin 2\varnothing + \sin 4\varnothing) \right] \tag{8}$$

It is interesting to see for symmetrically double-edge-cracked samples the revised stress intensity factor K_I^0 decreases as the increasing of inclined angle, however, the revised K_{II}^0 still keep the same value as $1.00K_{II}$, i.e., no change. As for anti-symmetrically double-edge-cracked samples both revised stress intensity factors, K_I^0 and K_{II}^0, decrease as the increasing of inclined angle; whilst, K_I^0 reduces from 1.00160 $K_{II}$for a = 2.0 mm, and $1.00421K_I$ for a = 3.0 mm at inclined angle 30°, i.e., K_I^0 is

over $1.0K_I$ at $\theta = 30°$, down to $0.99954K_I$ for a = 2.0 mm and $0.99890K_I$ for a = 3.0 mm at $\theta = 60°$, i.e., K_I^0 is lower than $1.0K_I$.

Based on the suitable methodology to predict crack growth rate and life the well-known Paris Law has to be modified. In the mixed mode fracture the effective revised stress intensity factor range, ΔK_e, instead of K_I^0 and K_{II}^0, the hybrid FMLs material properties and mechanical behavior, and most importantly the fracture process and mechanisms need be involved.

The surprising and interesting phenomenon is the occurrence of a small broken ellipse at the center part when both side crack tips grow towards each other along the shortest path to deviate slightly and do not coalesce. Due to their interaction, both crack tips run around each other in a certain distance until, at some later instant, each of them merges with the other crack. The failure mechanisms of nanocomposite symmetrically double-edge-cracked samples due to cyclic loading were shown in Figure 6(a) the enlarged scheme and Figure 6 (b) the photo of failed sample. Similarly, the failure mechanisms of nanocomposite anti-symmetrically double-edge-cracked samples due to cyclic loading were presented in Figure 7(a) the enlarged scheme and Figure 7(b) the photos of three failed samples.

Based on the above-mentioned the particular failure mechanisms such as the small elliptical pieces formed at failure in both kinds of FMLs that the irregular crack growth rate and path make the fatigue life prediction a very complicated task.

Comparing the fatigue lives of samples with symmetrically double-edged cracks with the counterpart of those of anti-symmetrically double-edged cracks it was obvious to see the lives of latter were slightly higher than the former since that the distance between two crack tips of the latter was a little bit longer than the former. From the different point of view if the samples of FMLs, i.e., Ti/APC-2, with

symmetrically double-edged cracks were cut into two halfs longitudinally, they became the samples with inclined single-edge crack of half width. The lives of both the samples with symmetrically double-edged cracks and those counterparts with inclined single-edge cracks [20] may be expected straightforwardly close to each other. However, some data of lives were actually very close, others were significantly scattered, please refer to Table 7. It is attributed the different boundary conditions, i.e., the inclined single-edge cracks grow directly towards the free edges; whilst, the symmetrically double-edged cracks propagate towards each other due to the interaction attraction of two crack tips. Additionally, the existing failure mechanism of a small piece of ellipse at the center results in the delay of sample broken, i.e., the retardation increases the lives of samples of symmetrically double-edged cracks.

5. CONCLUSION

The neat and nanocomposite Ti/APC-2 hybrid laminates were fabricated. Two types of symmetrical and anti-symmetrical double-edge-cracked specimens were made. The crack lengths were 2.0 mm and 3.0 mm and inclined angles θ = 30°, 45°, and 60° for symmetric samples and θ = ±30°, ±45°, and ±60° for anti-symmetric samples. All the specimens were subjected to tensile tests and cyclic tests separately to obtain the load-displacement curves and the mechanical properties, and the P-N curves and fatigue lives, respectively.

The longer the crack lengths are, the lower the properties and lives are. Similarly, the higher the inclined angles are, the lower the properties and live are. The enhancement of adding nano-powder did improve the mechanical properties, but not significantly. The mechanical properties and fatigue lives are better for anti-symmetric samples than those of symmetric samples. The failure mechanisms of small elliptical broken pieces were found due to cyclic loading for both kinds of FMLs.

ACKNOWLEDGEMENTS

The authors would like to gratefully acknowledge the sponsorship from the Ministry of Science and Technology under the project number: MOST 107-2221-E-110-051.

REFERENCES

1. Jen MHR, Chang CK and Sung YC. Fabrication and mechanical properties of Ti/ APC-2 hybrid nanocomposite laminates at elevated temperatures. *J Compos Mater* 2015;50: 2035-2045.
2. Jen MHR, Tseng YC and Li PY. Fatigue response of hybrid magnesium/carbon-fiber/PEEK nanocomposite laminates at elevated temperature. *J Jpn Soc Exp Mech* 2017;7: s56-s60.
3. Abdullah MR and Cantwell WJ. The impact resistance of polypropylene-based fibre-metal laminates. *Compos Sci Technol* 2006;66: 1682-1693.
4. Sinke J. Development of fibre metal laminates: concurrent multi-scale modeling and testing. *J Mater Sci* 2006;41: 6777-6788.
5. Liu Q, Ma J, Kang L, et al. An experimental study on fatigue characteristics of CFRP-steel hybrid laminates. *Master Design* 2015;88: 643-650.
6. Burianek DA and Spearing SM. Fatigue damage in titanium-graphite hybrid laminates. *Compos Sci Technol* 2002;62: 607-617.
7. Dadej K, Bienias J and Surowska B. Residual fatigue life of carbon fibre aluminum laminates. *Int J Fatigue* 2017;100(1): 94-104.
8. Alderliesten R. *Fatigue and fracture of fibre metal laminates*. New York, USA: Springer, 2017.
9. Gross D and Seelig T. *Fracture mechanics: with an introduction to micromechanics*. first ed. Berlin Heidelberg, Germany, 2006.
10. Aliha MRM, Mousavi SS, Bahmani A, et al. Crack initiation angles and

propagation paths in polyurethane foams under mixed mode I/II and I/III loading. *Theor Appl Fract Mech* 2019;101: 152-161.

11. Alderliesten RC. Analytical prediction model for fatigue crack propagation and delamination growth in GLARE. *Int J Fatigue* 2007;29: 628-646.
12. Guo YJ and Wu XR. Bridging stress distribution in center-cracked fiber reinforced metal laminates: modeling and experiment. *Eng Fract Mech* 1999;63: 147-163.
13. Chang P and Yang J. Modeling of fatigue crack growth in notched fiber metal laminates. *Int J Fatigue* 2008;30: 2165-2174.
14. Homan JJ. Fatigue initiation in fiber metal laminates. *Int J Fatigue* 2006;28: 366-374.
15. Gupta M. *Directionality of damage growth in fiber metal laminates and hybrid structures*. PhD Thesis, E.T.S.I.A. Universi dad Polytechnico de Madrid, 2015.
16. Wang HT, Wu G and Pang YY. Theoretical and numerical study on stress intensity factors for FRP- strengthened steel plates with double-edged cracks. *Sensor* 2018;18: E2356.
17. Jen MHR, Tseng YC and Wu CH. Manufacturing and mechanical response of nanocomposite laminates. *Compos Sci Technol* 2005;65: 775-779.
18. Muhammad Ilham K, Anuar H, Norhashimah MS, et al. Matrix cracking in reinforced polymer nanocomposites: a review. *J Adv Rev Sci Res* 2015;11: 13-36.
19. Borowski E, Soliman E, Kandi UF, et al. Interlaminar fracture toughness of CFRP laminates incorporating multi-walled carbon nanotubes. *Polymer* 2015;7: 1020-1045.
20. Jen MHR, Kuo GT, Wu YH, et al. Fatigue responses of cracked Ti/APC-2 nanocomposite laminates at elevated temperature. *J Compos Mater* 2019;54:

1705-1715.

Table 1(a). The mechanical properties of neat symmetrically double-edge-cracked composite laminates at θ =30°, 45°, and 60° for 2.0 mm crack length.

Sample No.	Ultimate Tensile Load P_{ult} (kN)	Max. Displacement Δ (mm)	Initial Compliance C_{11i} ($\frac{mm}{kN}$)	Secant Compliance C_{11s} ($\frac{mm}{kN}$)
		$\theta = 30°$		
Ti_2.0_30+30-1	12.52	2.205	0.06983	0.19067
Ti_2.0_30+30-2	13.51	2.142	0.08778	0.16977
Ti_2.0_30+30-3	13.11	2.163	0.05059	0.20581
Average	13.04±0.495	2.170±0.0315	0.06940±0.0186	0.18882±0.0180
		$\theta = 45°$		
Ti_2.0_45+45-1	13.36	2.079	0.05669	0.18965
Ti_2.0_45+45-2	14.39	2.184	0.07632	0.16587
Ti_2.0_45+45-3	14.29	2.373	0.09043	0.16962
Average	14.01±0.515	2.212±0.147	0.07790±0.0168	0.17138±0.0119
		$\theta = 60°$		
Ti_2.0_60+60-1	14.51	2.037	0.05877	0.1970
Ti_2.0_60+60-2	14.14	2.058	0.05824	0.1978
Ti_2.0_60+60-3	13.63	2.016	0.06147	0.2056
Average	14.09±0.44	2.037±0.021	0.05949±0.0016	0.2002±0.0043

Note:
C_{11i} (Initial Longitudinal Compliance): range $0.1 \leq \Delta \leq 0.28$.

C_{11s} (Secant Modulus Compliance): range $0.6 \leq \Delta \leq 1.5$.

Table 1(b). The mechanical properties of neat symmetrically double-edge-cracked composite laminates at θ =30°, 45°, and 60° for 3.0 mm crack length.

Sample No.	Ultimate Tensile Load P_{ult} (kN)	Max. Displacement Δ (mm)	Initial Compliance C_{11i} ($\frac{mm}{kN}$)	Secant Compliance C_{11s} ($\frac{mm}{kN}$)
		$\theta = 30°$		
Ti_3.0_30+30-1	12.43	2.331	0.05669	0.24359
Ti_3.0_30+30-2	11.59	2.415	0.07862	0.19810
Ti_3.0_30+30-3	12.75	2.268	0.04900	0.20305
Average	12.26±0.580	2.338±0.074	0.06143±0.0148	0.21491±0.0227
		$\theta = 45°$		
Ti_3.0_45+45-1	13.01	2.247	0.05838	0.22752
Ti_3.0_45+45-2	12.86	2.142	0.06250	0.21997
Ti_3.0_45+45-3	12.93	2.331	0.06116	0.23063
Average	12.93±0.075	2.240±0.094	0.06068±0.0206	0.22604±0.0533
		$\theta = 60°$		
Ti_3.0_60+60-1	13.95	2.100	0.06757	0.19105
Ti_3.0_60+60-2	13.60	2.373	0.05642	0.21440
Ti_3.0_60+60-3	14.03	2.226	0.05585	0.21653
Average	13.86±0.215	2.233±0.136	0.05995±0.0586	0.20733±0.0127

Note:
C_{11i} (Initial Longitudinal Compliance): range $0.1 \leq \Delta \leq 0.28$.

C_{11s} (Secant Modulus Compliance): range $0.6 \leq \Delta \leq 1.5$.

Table 2(a). The mechanical properties of nanocomposite symmetrically double-edge-cracked samples at θ =30°, 45°, and 60° for 2.0 mm crack length.

Sample No.	Ultimate Tensile Load P_{ult} (kN)	Max. Displacement Δ (mm)	Initial Compliance C_{11i} ($\frac{mm}{kN}$)	Secant Compliance C_{11s} ($\frac{mm}{kN}$)
		$\theta = 30°$		
TiSi_2.0_30+30-1	13.37	2.247	0.08843	0.19661
TiSi_2.0_30+30-2	14.10	2.436	0.07860	0.20470
TiSi_2.0_30+30-3	13.95	2.646	0.08034	0.18049
Average	13.80±0.365	2.443±0.199	0.08264±0.0491	0.19393±0.0121
		$\theta = 45°$		
TiSi_2.0_45+45-1	14.52	2.037	0.06892	0.17782
TiSi_2.0_45+45-2	14.56	2.541	0.07968	0.18203
TiSi_2.0_45+45-3	14.39	2.205	0.07240	0.18708
Average	14.49±0.085	2.261±0.252	0.07367±0.0538	0.18231±0.0463
		$\theta = 60°$		
TiSi_2.0_60+60-1	14.90	2.499	0.07042	0.20593
TiSi_2.0_60+60-2	15.53	2.583	0.07823	0.17422
TiSi_2.0_60+60-3	15.39	2.562	0.06566	0.17964
Average	15.27±0.315	2.548±0.042	0.07144±0.0628	0.18666±0.0158

Note:
C_{11i} (Initial Longitudinal Compliance): range $0.1 \leq \Delta \leq 0.28$.

C_{11s} (Secant Modulus Compliance): range $0.6 \leq \Delta \leq 1.5$.

Table 2(b). The mechanical properties of nanocomposite symmetrically double-edge-cracked samples at θ =30°, 45°, and 60° for 3.0 mm crack length.

Sample No.	Ultimate Tensile Load P_{ult} (kN)	Max. Displacement Δ (mm)	Initial Compliance C_{11i} ($\frac{mm}{kN}$)	Secant Compliance C_{11s} ($\frac{mm}{kN}$)
		$\theta = 30°$		
TiSi_3.0_30+30-1	13.37	2.772	0.09253	0.19545
TiSi_3.0_30+30-2	13.68	2.709	0.07095	0.19163
TiSi_3.0_30+30-3	13.26	2.688	0.08837	0.17011
Average	13.43±0.210	2.723±0.042	0.08395±0.0108	0.18573±0.0126
		$\theta = 45°$		
TiSi_3.0_45+45-1	14.10	2.751	0.07860	0.20470
TiSi_3.0_45+45-2	14.26	2.772	0.08638	0.17233
TiSi_3.0_45+45-3	13.89	2.709	0.08117	0.19687
Average	14.08±0.185	2.744±0.031	0.08205±0.0038	0.19130±0.0161
		$\theta = 60°$		
TiSi_3.0_60+60-1	14.64	2.709	0.06865	0.18636
TiSi_3.0_60+60-2	14.72	2.793	0.07174	0.18314
TiSi_3.0_60+60-3	14.19	2.730	0.06998	0.19414
Average	14.51±0.265	2.744±0.042	0.07012±0.0154	0.18788±0.0550

Note:
C_{11i} (Initial Longitudinal Compliance): range $0.1 \leq \Delta \leq 0.28$.

C_{11s} (Secant Modulus Compliance): range $0.6 \leq \Delta \leq 1.5$.

Table 3(a). The mechanical properties of neat anti-symmetrically double-edge-cracked samples at $\theta = \pm 30°$, $\pm 45°$, and $\pm 60°$ for 2.0 mm crack length.

Sample No.	Ultimate Tensile Load P_{ult} (kN)	Max. Displacement Δ (mm)	Initial Compliance C_{11i} ($\frac{mm}{kN}$)	Secant Compliance C_{11s} ($\frac{mm}{kN}$)
		$\theta = \pm 30°$		
Ti_2.0_30-30-1	14.39	2.331	0.08079	0.16568
Ti_2.0_30-30-2	14.66	2.226	0.06852	0.19664
Ti_2.0_30-30-3	14.63	2.205	0.08032	0.16278
Average	14.56±0.14	2.254±0.063	0.0765±0.0061	0.1750±0.0168
		$\theta = \pm 45°$		
Ti_2.0_45-45-1	14.35	2.331	0.05756	0.19888
Ti_2.0_45-45-2	14.60	2.352	0.06121	0.20960
Ti_2.0_45-45-3	14.76	2.289	0.05809	0.19189
Average	14.57±0.22	2.324±0.032	0.0589±0.0018	0.2001±0.0088
		$\theta = \pm 60°$		
Ti_2.0_60-60-1	14.54	2.205	0.06229	0.19606
Ti_2.0_60-60-2	14.70	2.016	0.05718	0.18760
Ti_2.0_60-60-3	14.73	2.247	0.05742	0.19396
Average	14.66±0.10	2.156±0.115	0.0590±0.0025	0.1925±0.0042

Note:

C_{11i} (Initial Longitudinal Compliance): range $0.1 \leq \Delta \leq 0.28$.

C_{11s} (Secant Modulus Compliance): range $0.6 \leq \Delta \leq 1.5$.

Table 3(b). The mechanical properties of neat anti-symmetrically double-edge-cracked samples at $\theta = \pm 30°$, $\pm 45°$, and $\pm 60°$ for 3.0 mm crack length.

Sample No.	Ultimate Tensile Load P_{ult} (kN)	Max. Displacement Δ (mm)	Initial Compliance C_{11i} ($\frac{mm}{kN}$)	Secant Compliance C_{11s} ($\frac{mm}{kN}$)
		$\theta = \pm 30°$		
Ti_3.0_30-30-1	12.02	2.373	0.07986	0.19883
Ti_3.0_30-30-2	12.55	2.436	0.08403	0.19097
Ti_3.0_30-30-3	11.77	1.953	0.07130	0.21040
Average	12.11±0.39	2.254±0.241	0.0784±0.0636	0.2001±0.0971
		$\theta = \pm 45°$		
Ti_3.0_45-45-1	13.10	2.310	0.05942	0.22027
Ti_3.0_45-45-2	13.17	2.226	0.08638	0.17157
Ti_3.0_45-45-3	12.39	2.331	0.07816	0.19486
Average	12.88±0.39	2.289±0.052	0.0747±0.0269	0.1956±0.0243
		$\theta = \pm 60°$		
Ti_3.0_60-60-1	13.75	2.226	0.06023	0.21765
Ti_3.0_60-60-2	14.23	2.058	0.05723	0.20279
Ti_3.0_60-60-3	13.37	1.806	0.05566	0.19782
Average	13.78±0.43	2.030±0.210	0.0577±0.0228	0.2061±0.0991

Note:

C_{11i} (Initial Longitudinal Compliance): range $0.1 \leq \Delta \leq 0.28$.

C_{11s} (Secant Modulus Compliance): range $0.6 \leq \Delta \leq 1.5$.

Table 4(a). The mechanical properties of nanocomposite anti-symmetrically double-edge-cracked samples at $\theta = \pm 30°$, $\pm 45°$, and $\pm 60°$ for 2.0 mm crack length.

Sample No.	Ultimate Tensile Load P_{ult} (kN)	Max. Displacement Δ (mm)	Initial Compliance C_{11i} ($\frac{mm}{kN}$)	Secant Compliance C_{11s} ($\frac{mm}{kN}$)
		$\theta = \pm 30°$		
TiSi_2.0_30-30-1	13.36	2.394	0.07783	0.20089
TiSi_2.0_30-30-2	14.10	2.709	0.09891	0.17350
TiSi_2.0_30-30-3	14.25	2.667	0.08759	0.17186
Average	13.90±0.46	2.590±0.157	0.0881±0.0105	0.1821±0.0145
		$\theta = \pm 45°$		
TiSi_2.0_45-45-1	14.12	2.394	0.06340	0.18480
TiSi_2.0_45-45-2	14.43	2.331	0.09252	0.17704
TiSi_2.0_45-45-3	14.97	2.793	0.08184	0.17286
Average	14.50±0.43	2.506±0.231	0.0797±0.0291	0.1782±0.0597
		$\theta = \pm 60°$		
TiSi_2.0_60-60-1	15.50	2.625	0.08336	0.17101
TiSi_2.0_60-60-2	15.65	2.835	0.06059	0.22139
TiSi_2.0_60-60-3	14.91	2.289	0.05572	0.19434
Average	15.35±0.37	2.583±0.273	0.0666±0.0138	0.1959±0.0251

Note:
C_{11i} (Initial Longitudinal Compliance): range $0.1 \leq \Delta \leq 0.28$.

C_{11s} (Secant Modulus Compliance): range $0.6 \leq \Delta \leq 1.5$.

Table 4(b). The mechanical properties of nanocomposite anti-symmetrically double-edge-cracked samples at $\theta = \pm 30°$, $\pm 45°$, and $\pm 60°$ for 3.0 mm crack length.

Sample No.	Ultimate Tensile Load P_{ult} (kN)	Max. Displacement Δ (mm)	Initial Compliance C_{11i} ($\frac{mm}{kN}$)	Secant Compliance C_{11s} ($\frac{mm}{kN}$)
		$\theta = \pm 30°$		
TiSi_3.0_30-30-1	12.44	2.541	0.09937	0.19459
TiSi_3.0_30-30-2	12.07	2.436	0.08237	0.20423
TiSi_3.0_30-30-3	12.68	2.730	0.09910	0.19860
Average	12.40±0.32	2.569±0.147	0.0936±0.0085	0.1991±0.0048
		$\theta = \pm 45°$		
TiSi_3.0_45-45-1	13.57	2.730	0.07402	0.19563
TiSi_3.0_45-45-2	13.44	2.415	0.09162	0.17509
TiSi_3.0_45-45-3	13.42	2.625	0.10406	0.19219
Average	13.48±0.08	2.590±0.157	0.0899±0.0151	0.1876±0.0102
		$\theta = \pm 60°$		
TiSi_3.0_60-60-1	14.28	2.667	0.09258	0.17359
TiSi_3.0_60-60-2	14.06	2.457	0.08239	0.20689
TiSi_3.0_60-60-3	14.03	2.520	0.06908	0.17714
Average	14.12±0.13	2.548±0.105	0.0814±0.0117	0.1859±0.0166

Note:
C_{11i} (Initial Longitudinal Compliance): range $0.1 \leq \Delta \leq 0.28$.

C_{11s} (Secant Modulus Compliance): range $0.6 \leq \Delta \leq 1.5$.

Table 5. The revised results of stress intensity factors for nanocomposite symmetrically double-edge-cracked samples of two crack lengths at each inclined angle.

Crack Length a (mm)	Crack Angle $\alpha=\beta$ (degree)	Length a (mm)	Angle ϕ (degree)	Length d (mm)	K_I^0 $\left(MPa\sqrt{m}\right)$	K_{II}^0 $\left(MPa\sqrt{m}\right)$
2	30	1	0	21.54	1.001078 K_I	$1.00K_{II}$
	45		0	22.17	1.001017 K_I	$1.00K_{II}$
	60		0	23.00	1.000945 K_I	$1.00K_{II}$
3	30	1	0	19.80	1.002870 K_I	$1.00K_{II}$
	45		0	20.76	1.002610 K_I	$1.00K_{II}$
	60		0	22.00	1.002324 K_I	$1.00K_{II}$

Table 6. The revised results of stress intensity factors for nanocomposite anti-symmetrically double-edge-cracked samples of two crack lengths at each inclined angle.

Length a (mm)	Crack Angle θ	Length d (mm)	Length e (mm)	Angle ϕ (degree)	K_I^0 $\left(MPa\sqrt{m}\right)$	K_{II}^0 $\left(MPa\sqrt{m}\right)$
1.0	30°	21.63	23.27	5.31°	$1.00160K_I$	$1.00000K_{II}$
	45°	22.35	23.59	7.27°	$1.00100K_I$	$0.99900K_{II}$
	60°	23.26	24.00	8.57°	$0.99954K_I$	$0.99840K_{II}$
1.5	30°	20.03	22.40	8.61°	$1.00421K_I$	$1.00000K_{II}$
	45°	21.19	23.94	11.55°	$1.00251K_I$	$0.99749K_{II}$
	60°	22.61	24.25	13.29°	$0.99890K_I$	$0.99619K_{II}$

Table 7. The fatigue lives of samples with inclined single-edge cracks and symmetrically double-edged cracks in contrast.

	The lives of nanocomposite FMLs with inclined single-edge cracks at 100°C*		The lives of nanocomposite FMLs with symmetrically double-edged cracks at RT	
Normalized applied maximum load P_{max}/P_{ult}	Inclined angles, α		Inclined angles, $\alpha=\beta$	
	45°	60°	45°	60°
	N_f (Cycles)	N_f (Cycles)	N_f (Cycles)	N_f (Cycles)
0.9	66	336	358	258
0.8	388	937	1,572	1,333
0.7	9,800	53,226	9,851	8,655

Note: * The part of data taken from reference [20]

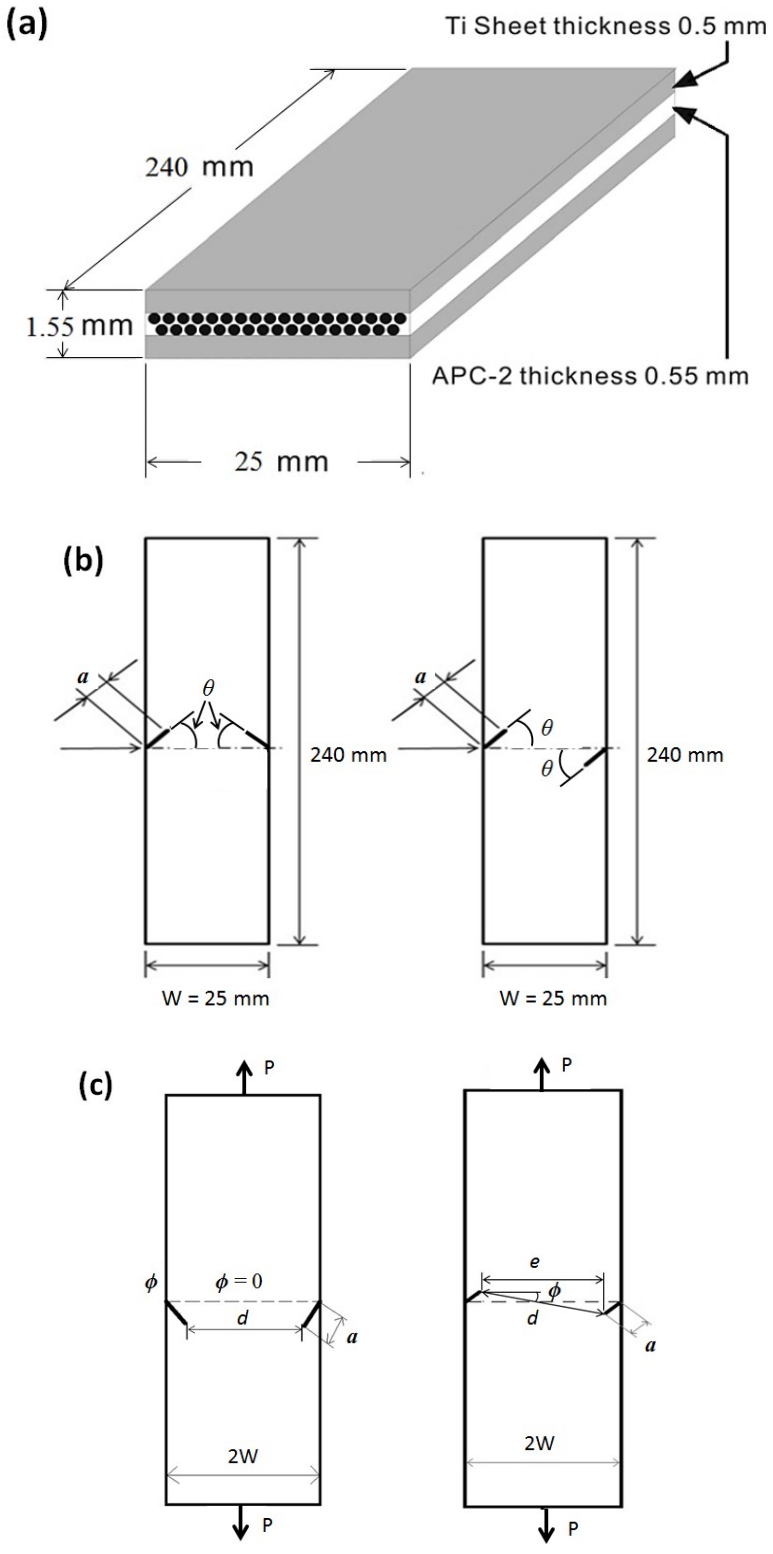

Figure 1. The scheme of (a) geometry and dimensions of nanocomposite laminate and (b) geometry of double-edge-cracked sample such as symmetrically, left and anti-symmetrically, right, (c) the distance between two crack tips.

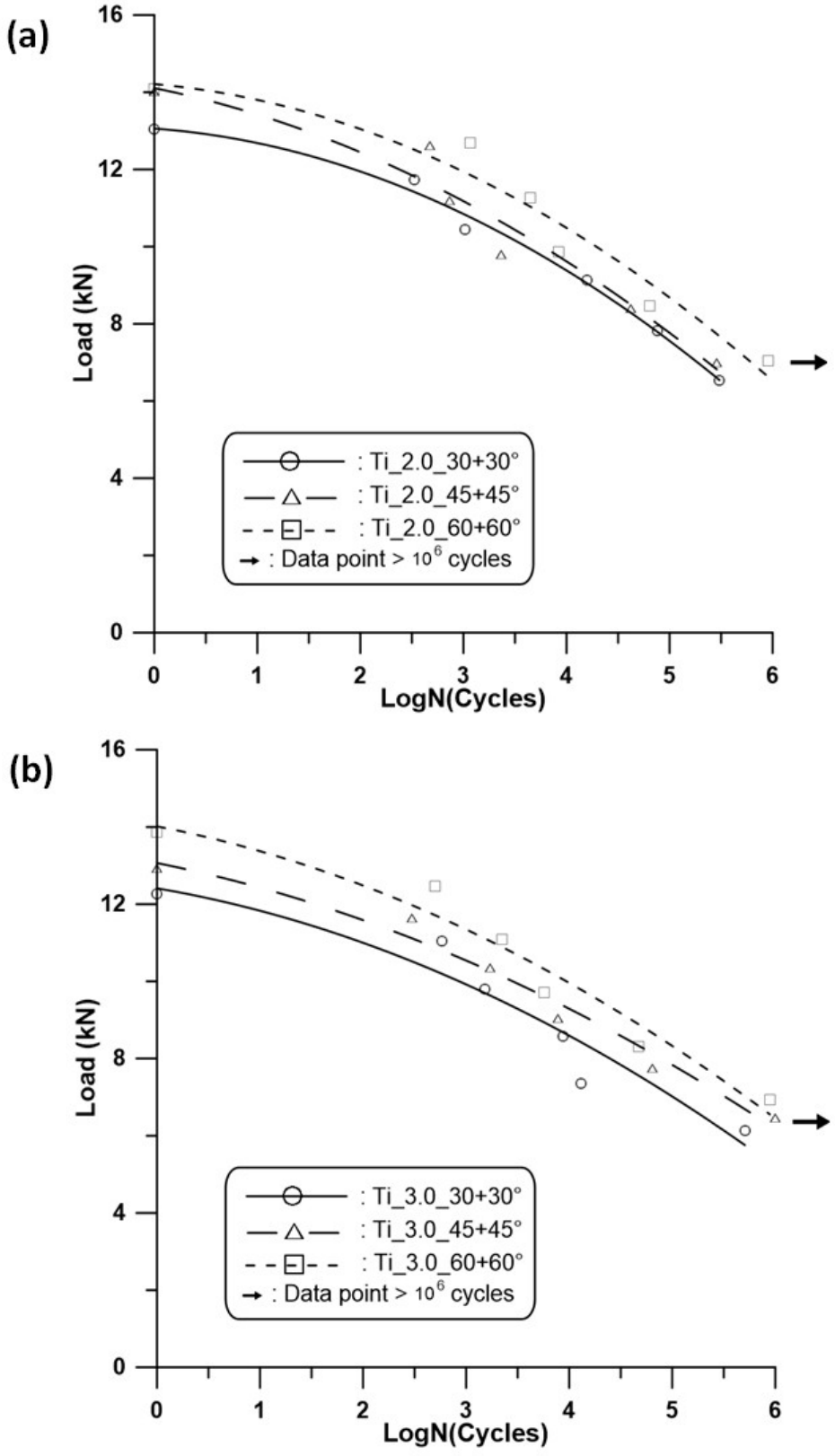

Figure 2. The P-N curves for neat symmetrically double-edge-cracked samples θ = 30°, 45° and 60° for (a) crack length 2 mm and (b) crack length 3 mm.

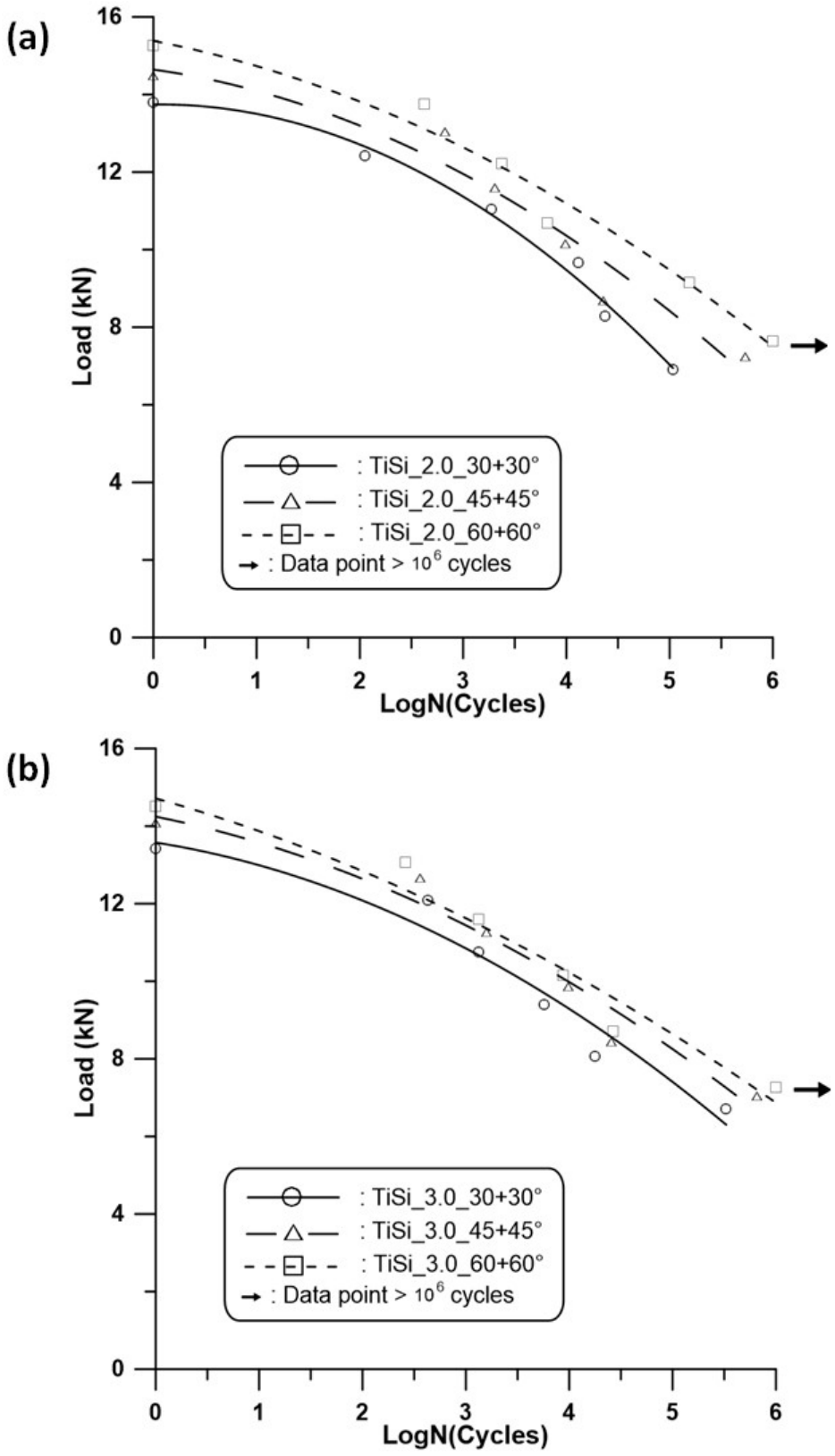

Figure 3. The P-N curves for nanocomposite symmetrically double-edge-cracked samples $\theta = 30°$, 45° and 60° for (a) crack length 2 mm and (b) crack length 3 mm.

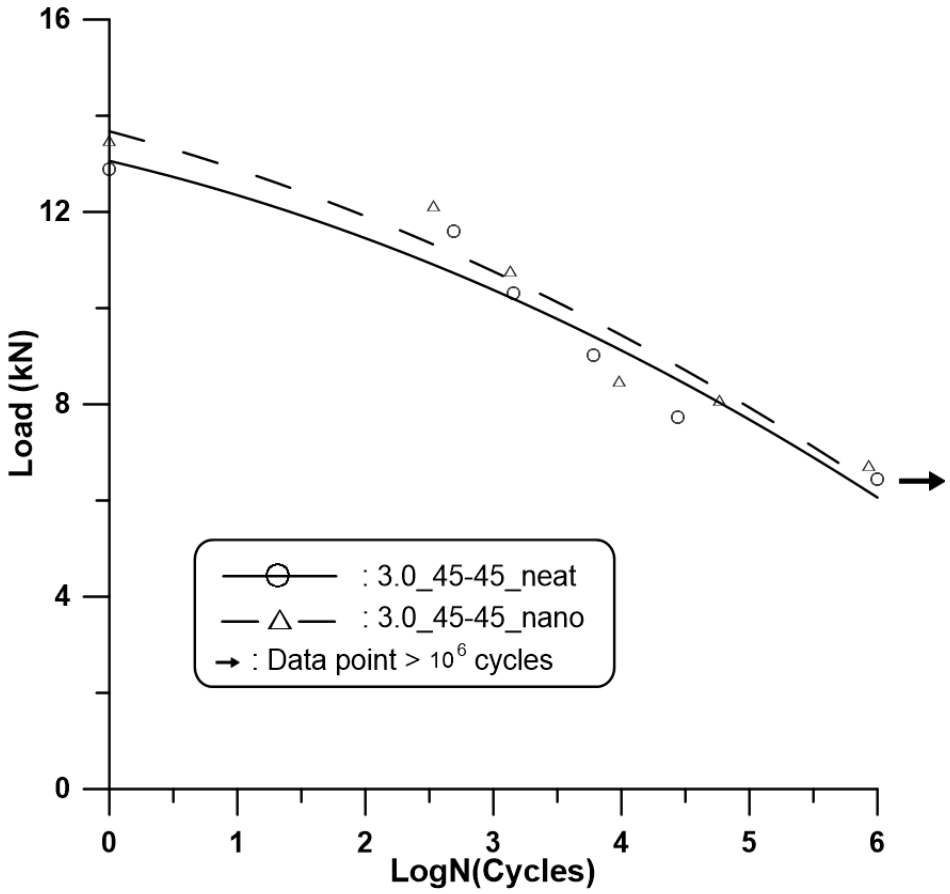

Figure 4. The P-N curves for both neat and nanocomposite anti-symmetrically double-edge-cracked samples of crack length 3.0 mm and $\theta = \pm 45°$.

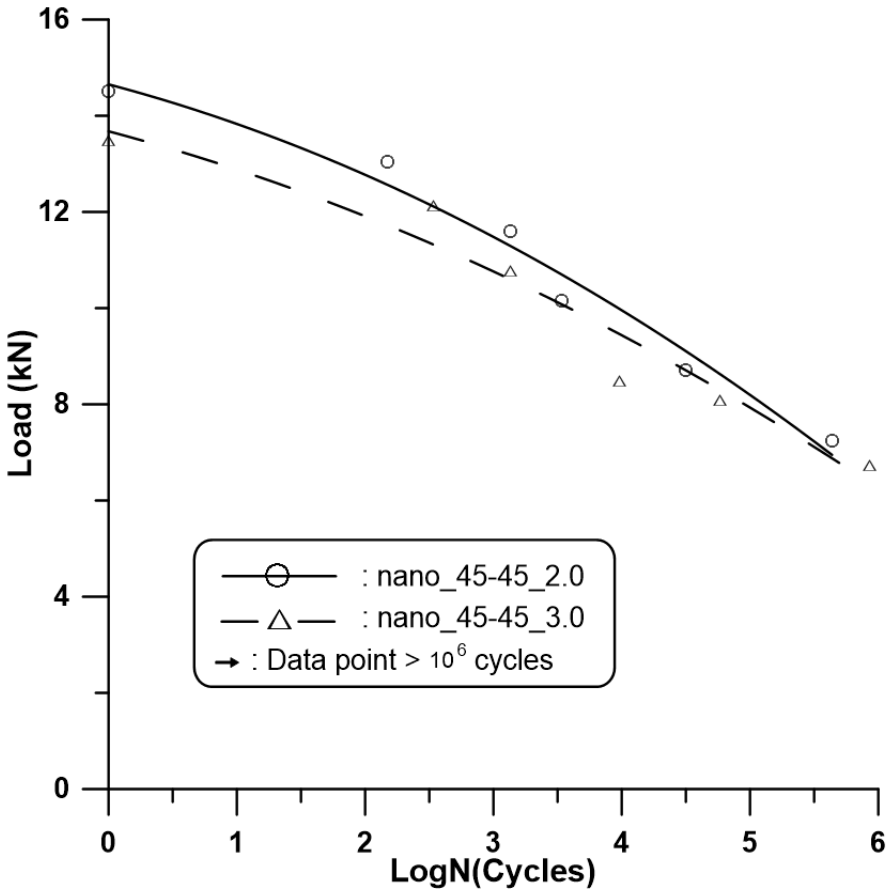

Figure 5. The P-N curves for 2.0 and 3.0 mm crack lengths in nanocomposite anti-symmetrically double-edge-cracked samples $\theta = \pm 45°$.

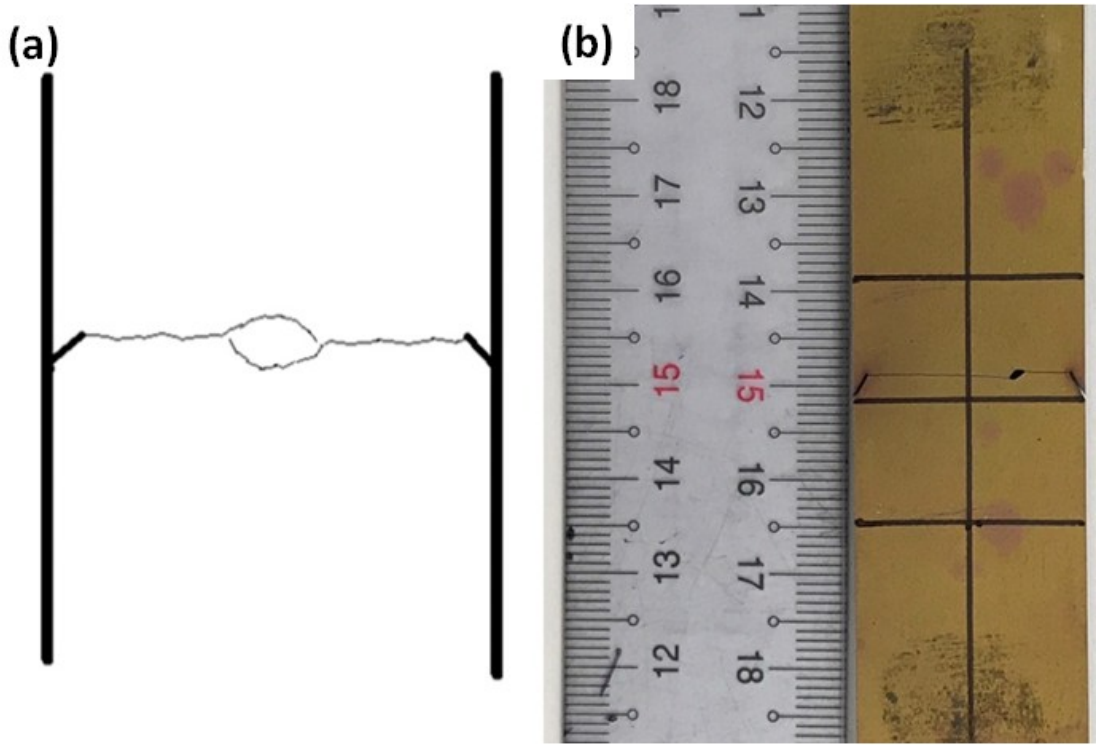

Figure 6. The failure mechanisms of symmetrically double-edge-cracked samples due to cyclic loading (a) the enlarged scheme and (b) the photo of failed sample.

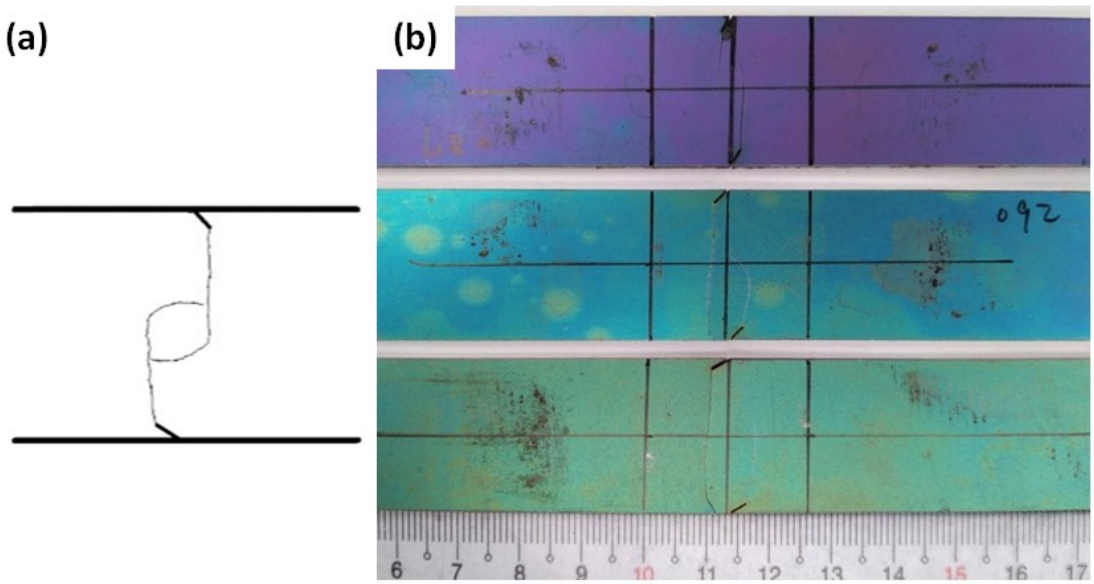

Figure 7. The failure mechanism of anti-symmetrically double-edge-cracked samples due to cyclic loading (a) the enlarged scheme and (b) the photos of three failed samples.